Porous Gold Films Fabricated by Wet-Chemistry Processes

Aymeric Pastre, Odile Cristini, Alexandre Boé, Katarzyna Raulin, Bertrand Grimbert, Fernand Chassagneux, Nathalie Rolland, Remy Bernard

Hindawi Publishing Corporation
Journal of Nanomaterials
Volume 2016, Article ID 3536153, 9 pages
http://dx.doi.org/10.1155/2016/3536153

Research Article

Porous Gold Films Fabricated by Wet-Chemistry Processes

Aymeric Pastre,[1] Odile Cristini,[2] Alexandre Boe,[1] Katarzyna Raulin,[1] Bertrand Grimbert,[1] Fernand Chassagneux,[3] Nathalie Rolland,[4] and Remy Bernard[2]

[1]*Institut d'Electronique de Microélectronique et de Nanotechnologie (IEMN), CNRS, UMR 8520, Université Lille 1, 59658 Villeneuve d'Ascq Cedex, France*
[2]*Physique des Lasers Atomes et Molécules (PhLAM), CNRS, UMR 8523, Université Lille 1, 59655 Villeneuve d'Ascq Cedex, France*
[3]*Laboratoire des Multimatériaux et Interfaces (LMI), CNRS, UMR 5615, Université Lyon 1, 69622 Villeurbanne Cedex, France*
[4]*Institut de Recherche sur les Composants Logiciels et Matériels pour l'Information et la Communication Avancée (IRCICA), CNRS, USR 3380, Université Lille 1, 59658 Villeneuve d'Ascq Cedex, France*

Correspondence should be addressed to Aymeric Pastre; aymeric.pastre@univ-lille1.fr

Received 5 November 2015; Revised 29 January 2016; Accepted 7 February 2016

Academic Editor: Gurvinder Singh

Porous gold films presented in this paper are formed by combining gold electroless deposition and polystyrene beads templating methods. This original approach allows the formation of conductive films (2×10^6 $(\Omega{\cdot}\mathrm{cm})^{-1}$) with tailored and interconnected porosity. The porous gold film was deposited up to 1.2 μm on the silicon substrate without delamination. An original zirconia gel matrix containing gold nanoparticles deposited on the substrate acts both as an adhesion layer through the creation of covalent bonds and as a seed layer for the metallic gold film growth. Dip-coating parameters and gold electroless deposition kinetics have been optimized in order to create a three-dimensional network of 20 nm wide pores separated by 20 nm thick continuous gold layers. The resulting porous gold films were characterized by GIXRD, SEM, krypton adsorption-desorption, and 4-point probes method. The process is adaptable to different pore sizes and based on wet-chemistry. Consequently, the porous gold films presented in this paper can be used in a wide range of applications such as sensing, catalysis, optics, or electronics.

1. Introduction

The combination of the intrinsic properties of gold and of those of a porous material makes porous gold films (PGFs) an interesting material in many applications. These films are conductive [1] and chemically stable [2], present good wettability in electrolyte solutions [3], and exhibit a large specific surface area. Thus, porous gold films are increasingly used for electrochemical devices such as electric double-layer capacitors (EDLC) [4–7], Li-ion batteries [4, 8], or fuel cells [9, 10]. PGFs are also used as bio/chemical sensing electrode systems [2, 11–14], based on their nontoxic and biocompatible nature [12] and on the presence of active sites for biomaterials. In addition, these films present a high electrocatalytic activity, rapid mass transport, and a good thermal stability, which makes them suitable for (electro)catalytic applications [12, 15–17]. Finally, PGFs exhibit excellent properties concerning Surface-Enhanced Raman Spectroscopy (SERS), Fluorescence, and Surface Plasmon Resonance (SPR), making them an attractive material for optical applications [18–20].

The pore size (from the nm to the mm scale), the pore modality (mono- or multimodal), and the presence of accessible and interconnected pores are essential parameters to be taken into account in relation to the targeted application. Some applications require small pore sizes (nm scale) in order to have a large specific surface area and thus increasing the active surface of the material. On the other hand, some other applications need large pore sizes (μm scale) to ensure a better mass transport [14, 21, 22]. Developing processes to fabricate porous gold films with tailorable properties is of undeniable interest.

PGFs are currently fabricated using mainly either a top-down dealloying method or a bottom-up templating method. The dealloying process consists in selectively etching the less-noble metal from a binary alloy (mostly Ag_xAu_{1-x}) [11, 23].

The alloy is either directly bought from a supplier in the form of a metallic ribbon [6, 10, 18, 24] or fabricated using mainly cosputtering deposition [1, 5, 25, 26], electrodeposition [4, 9, 19], vapor/thermal deposition [22, 27, 28], or more rarely electroless deposition [15, 29]. The sample is then chemically or electrochemically selectively etched, leading to the formation of a porous framework of the remaining metal, composed of metallic ligaments and pore channels [23, 29]. Porous gold films fabricated by this method are tunable in thickness and pore size but present some weaknesses. First of all, they mostly require costly dedicated equipment and/or conductive substrate for the binary alloy fabrication (sputtering or electrodeposition methods). Then, the films are not systematically deposited on substrates, which could limit the scope of application. If deposited on substrates they require costly and constraining sputtering of Cr/Au or Ta/Au adhesion layers in order to prevent delamination of the film during etching [26]. Moreover, the dealloying process requires concentrated acid treatments to remove the less-noble metal from the alloy. The dealloyed films often contain some remains of this less-noble metal, degrading their catalytic properties [16]. Finally, PGFs contain pore sizes within the nm range, limited by the size of the less-noble metal aggregates composing the alloy. The templating method, on the other hand, is a simple and cost-effective way to create porous gold films of controlled pore sizes (from nm to μm scale) [17, 30]. This technique allows the formation of a porous film of a controlled thickness by a totally wet approach. It is based on the deposition of an assembly of spherical particles (template), followed by the filling of the interstitial spaces between the spheres by the material of our choice (which is gold here). The final step consists in removing the template (either by calcination or by dissolution (solvent or acid)), revealing the porous structure of the filling material. Various types of templates exist, allowing us to choose the pore sizes desired (from the nm to the mm scale): colloidal crystals (e.g., silica spheres) [31, 32], polymers (e.g., polystyrene beads) [15, 33–35], surfactants [13, 14, 36], hydrogen [21, 37], or biomaterials [38, 39]. Filling the interstices between the spheres is mainly achieved by electrodeposition method [13, 21, 32, 34, 37], which consists in an electrochemical growth of a selected metal on a conductive substrate. A variant of electrodeposition is the electroless deposition technique. It allows depositing metallic films, while avoiding the constraining use of a conductive substrate. Only a few papers [14, 31, 33, 35] are reporting the combined use of electroless deposition method and templating technique to create porous gold films so far.

In this paper, we present an original totally wet-chemistry approach to fabricate gold films with controlled and interconnected porosity using alternate of templating and electroless deposition processes. PS beads have been used here as template, since they allow the tailoring of the pores and are highly monodisperse, easily autoassembled, and easily removable. Gold electroless deposition method has been chosen to embed the PS beads in this conductive metal as we are able to control the thickness of the deposited film. An original Au/ZrO_2 film is deposited on a silicon substrate. It is composed of a zirconia (ZrO_2) gel matrix embedding gold nanoparticles. The inorganic matrix anchors the gold nanoparticles to the substrate. It creates Si-O-Zr bridges with the functionalized silicon substrate surface as a replacement for organic linkers previously reported in the literature [40]. The gold nanoparticles act as growth seeds for the growth of the gold film. Electrical, chemical, and structural properties of such films have been investigated during this work.

2. Materials and Methods

All the materials were purchased from Sigma-Aldrich (France). To avoid any purification, deoxygenated milli-Q water (18.2 MΩ·cm) was used in all the preparations. All reactions were carried out under argon atmosphere. All the glassware dedicated to the gold nanoparticles embedded in zirconia matrix synthesis is washed with aqua regia prior to use. $3 \times 2\,cm^2$ P-doped (5–10 Ω) pieces of Si (100) wafers are used as substrates. First, they are thermally oxidized (110°C) creating a 200 nm thick SiO_2 layer.

2.1. Preparation of the Au/ZrO_2 Sol. The gold nanoparticles embedded in zirconia matrix (Au/ZrO_2) were synthesized according to a previous work [41]. A solution containing equimolar (0.011 mol) amount of zirconium(IV) propoxide solution ($Zr(OC_3H_7)_4$, 70 wt.% in 1-propanol) and acetylacetone ($CH_3COCH_2COCH_3$, ≥99%) was prepared into a 250 mL three-necked flask. The mixture was stirred for 30 minutes under air to ensure the homogeneity of the solution and to allow the protection of the zirconium alkoxide by chelation with a β-diketone (acetylacetone) in order to slow down hydrolysis reaction [42]. 1 mM Gold(III) chloride trihydrate ($HAuCl_4{\cdot}3H_2O$, ≥99.9% trace metal basis) in 2-propanol ($(CH_3)_2CHOH$ absolute, over molecular sieve, ≥99.5%) gold solution and 13 mM of sodium borohydride ($NaBH_4$, ≥96%) in a mixture of water/2-propanol reducing agent solution were prepared on a side. The gold solution was added into the flask, and after a few minutes of stirring, the reducing agent solution was added under vigorous stirring. The yellowish solution takes instantly a blood-red colour. The stirring of the solution was carried on during 3 hours under air. Hexane ($CH_3(CH_2)_4CH_3$ anhydrous, ≥95%) was added to the Au/ZrO_2 sol and was centrifuged at 2500 rpm during 30 min at 0°C. The upper organic phase was thrown out and the Au/ZrO_2 solid phase redispersed in ethanol (CH_3CH_2OH absolute, ≥99.8%). DLS measurements and TEM analyses showed that the gold nanoparticles formed are approximately 5 nm in diameter.

2.2. Preparation of the PS Beads. The PS beads were synthesized by a modified microemulsion polymerization method [43]. 1 g of sodium dodecyl sulfate ($CH_3(CH_2)_{11}OSO_3Na$, ≥99.0%) is dissolved in 90 mL of water in a 250 mL three-necked flask topped with a reflux condenser and connected to argon. The temperature is raised to 80°C and 0.15 g of potassium persulfate ($K_2S_2O_8$, ≥99.0%) dissolved in 10 mL of water is added to the reaction batch. A mixture of 1.5 g of styrene ($C_6H_5CHCH_2$, ≥99%) and 0.1 g of 1-butanol ($CH_3(CH_2)_3OH$, ≥99.4%) is added drop by drop under mild

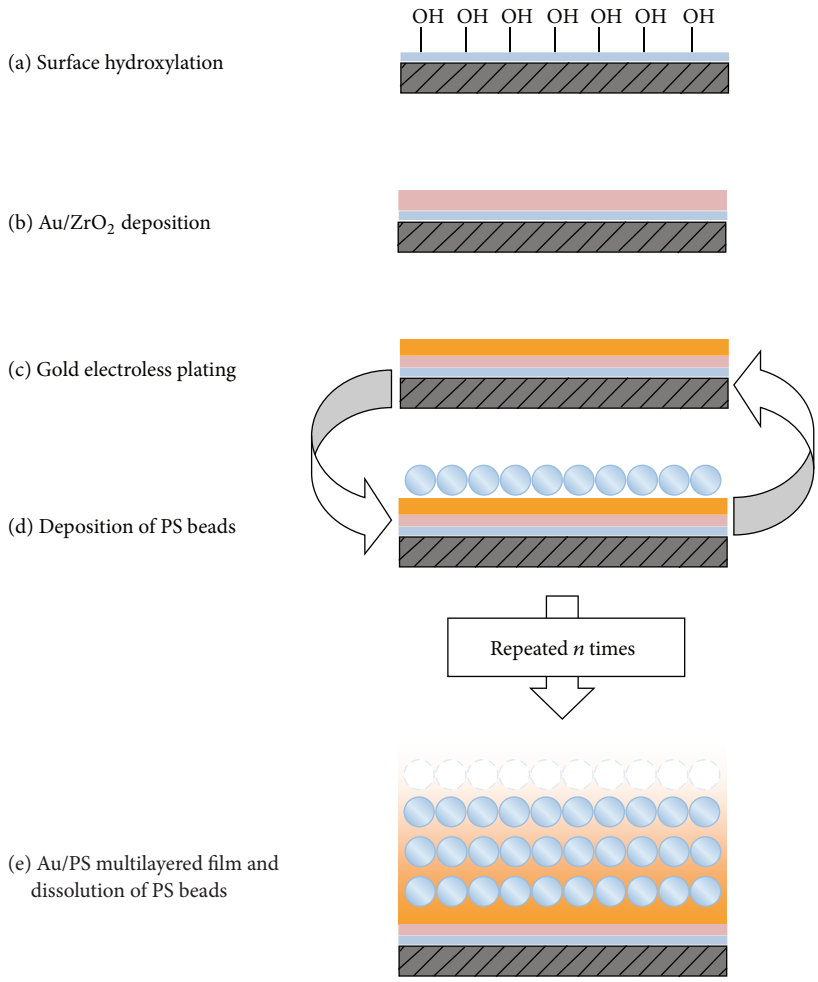

Figure 1: Schematic diagram of the porous gold film fabrication.

agitation (200 rpm) for 30 min. Then, 3.5 g of styrene is added all at once to the batch and is stirred for 1 hour. The solution is heated at 85°C for 1 hour before being cooled down to room temperature (RT). The bluish solution contains PS beads with a diameter of about 20 nm (determined by DLS measurements).

2.3. Fabrication of the Porous Gold Film. The fabrication process of such a film includes five steps. These steps are presented in Figure 1 and will be detailed in the following subsections.

2.3.1. Surface Hydroxylation. The oxidized silicon substrate is cleaned by soaking in a Piranha solution during 2 hours at RT followed by the immersion in a boiling solution containing hydrogen peroxide solution (H_2O_2, 30 wt.% in H_2O) and a few drops of ammonium hydroxide solution (NH_4OH, 28–30% NH_3 basis). This cleaning process allows the creation of hydroxyl groups on the surface of the silicon substrate (Figure 1(a)). The substrates can be stored in mQ-water until used (up to a month) [44].

2.3.2. Au/ZrO_2 Seed Layer Deposition. The seed layer, avoiding delamination of the film and containing gold nanoparticles, is deposited by dip-coating technique. The functionalized substrate is rinsed with mQ-water and dried vertically in air at RT. It is immersed in the Au/ZrO_2 stock solution during 10 s and withdrawn at a constant speed of 100 mm·min^{-1}. The substrates are dried vertically in air at RT for 2 hours (Figure 1(b)). The Au/ZrO_2 film, after the deposition and drying processes, has a bluish tint and is about 300 nm thick.

2.3.3. Gold Electroless Plating. The Au/ZrO_2-coated silicon substrate is immersed in an aqueous solution containing 4 mL of the ionic gold precursor ($HAuCl_4$, 0.1 wt.%) and 0.25 mL of hydrogen peroxide solution (H_2O_2, 30 wt.% in H_2O) for 2 minutes while agitated continuously. The Au/ZrO_2 film takes progressively a violet and then black colour. Finally, a goldish tint appears on the film (Figure 1(c)).

2.3.4. Deposition of the PS Beads Template. The PS beads were assembled on the gold-coated substrate by dip-coating method. The sample was immersed in the PS stock solution

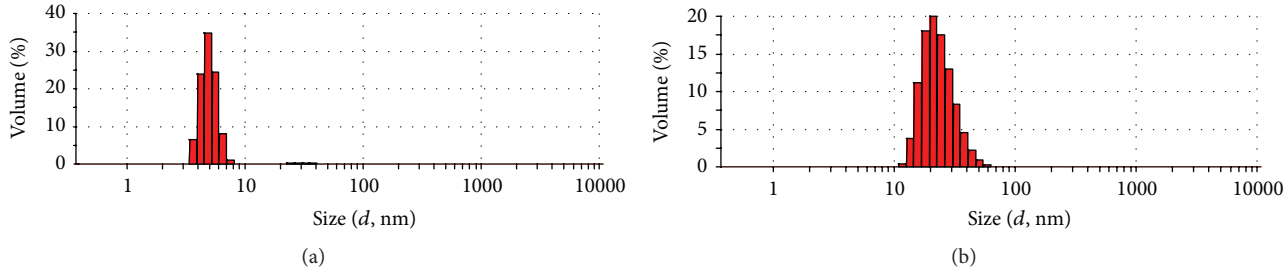

Figure 2: Size distribution by volume of (a) diluted ethanolic solution of Au/ZrO_2 and (b) diluted aqueous solution of PS beads.

for 10 min and withdrawn at a constant speed of 2 mm·min^{-1}. It is dried vertically in air at RT overnight [45]. The film deposited is opalescent and colourless (Figure 1(d)).

2.3.5. Au/PS Multilayered Film and Dissolution of PS Beads. The gold electroless plating and the deposition of the PS beads template steps were reproduced n times to form a multilayered film. The sample is finally immersed in toluene ($C_6H_5CH_3$, ≥95%) for 1 hour to remove the PS beads and create consequently porosity within the film (Figure 1(e)).

3. Results and Discussion

3.1. DLS Analysis. To determine the particle size and size distribution of the gold nanoparticles, Dynamic Light Scattering (DLS) analyses were performed using a Malvern Zetasizer Nano-S90 on diluted samples. The size distribution is expressed by volume, and the particle size is calculated as the average value of three successive measurements. The results represented below indicate that the ethanolic solution of Au/ZrO_2 contains gold nanoparticles with a mean diameter of 4.9 nm. The distribution is comprised between 2 nm and 8 nm with a maximum centered on 4.9 nm (Figure 2(a)). The solution is considered to be monodisperse in size since the peak is narrow. The same analyses have been conducted on a diluted aqueous solution of PS beads. The sample is monodisperse in size with a mean diameter of the bead equal to 26.1 nm (Figure 2(b)).

Polystyrene beads used as templates present the advantages of being tunable in size [46] (from 20 nm [43] to 400 nm [47]) and easily removable by soaking in toluene. They allow choosing the size of the pores created in our material according to the considered application while preserving their internal structure. The withdrawal speed chosen allows the formation of an assembly of polystyrene beads on the surface of the gold-coated sample. It is indeed observable on the inset of Figure 5(a) as the porous network is well-organized within the final material.

3.2. TEM Analysis. High Resolution Transmission Electron Microscopy (HRTEM) was carried out using a TOPCON EM002B TEM, operating at 200 kV. The TEM analysis performed on a diluted sample of Au/ZrO_2 confirms the size of the gold nanoparticles contained in the ethanolic solution (Figure 3). It shows as well that spherical gold nanoparticles

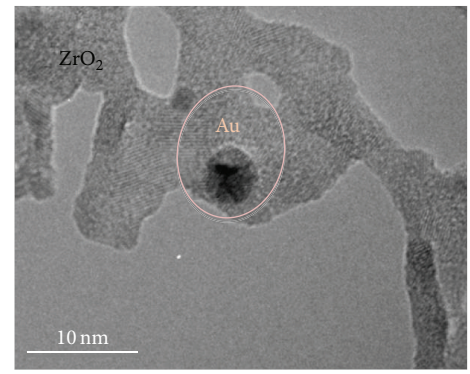

Figure 3: TEM picture of a gold nanoparticle embedded in zirconia matrix.

are indeed embedded in a zirconia matrix (light-grey in the picture).

3.3. Formation Mechanism of the Gold Film by Electroless Plating. The deposition of the Au/ZrO_2 seed layer by dip-coating technique allows us to control the thickness and the mechanical properties of the film. The withdrawal speed and the drying process are the main parameters to control in order to do this. The withdrawal speed chosen (100 mm·min^{-1}) allowed us to obtain the appropriate thickness of the film (300 nm). The film is uniformly deposited and continuous. The drying process (2 hours in air at RT) avoids the presence of cracks in the film and the delamination of the film. Gold nanoparticles are immobilized onto the silicon substrate thanks to the creation of strong Si-O-Zr bridges between the hydroxylated silica surface and the ZrO_2 matrix embedding these nanoparticles [42]. The H_2O_2 introduced during the electroless plating process acts as a reducing agent. It reduces the Au^{3+} from the ionic gold precursor ($HAuCl_4$) into Au^0 (reaction (3)) as explained in previous work [40]:

$$2AuCl_4^- + 6e^- \rightleftharpoons 2Au + 8Cl^- \quad (1)$$

$$3H_2O_2 \rightleftharpoons 3O_2 + 6H^+ + 6e^- \quad (2)$$

$$2AuCl_4^- + 3H_2O_2 \longrightarrow 2Au + 3O_2 + 8Cl^- + 6H^+ \quad (3)$$

Gold atoms (Au^0) reduced by the H_2O_2 in the gold plating bath contribute to the growth of the gold nanoparticles immobilized onto the substrate. These nanoparticles act

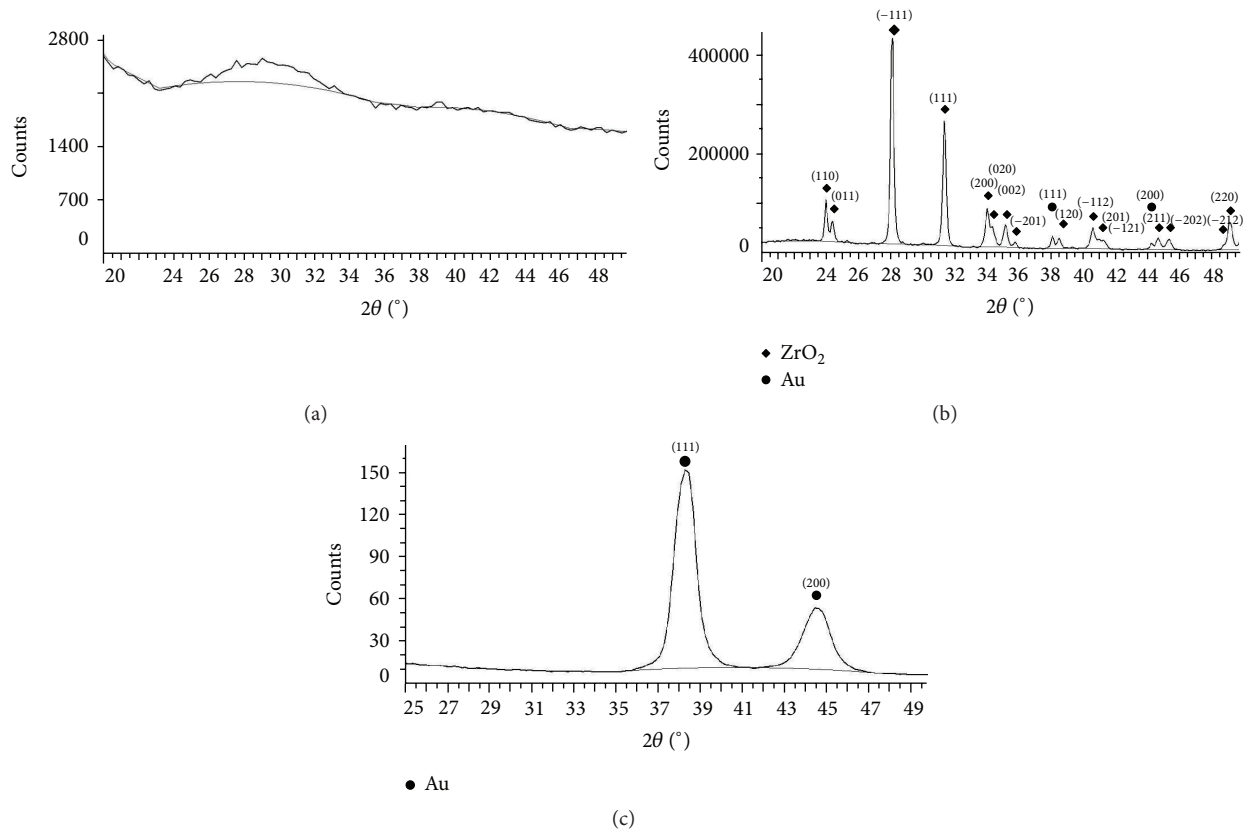

Figure 4: GIRDX diagrams of (a) amorphous Au/ZrO_2 at RT, (b) crystallized Au/ZrO_2 treated thermally at 1200°C, and (c) Au/PS 10-layered film.

as nucleation sites. Particles growth is followed by their coalescence to form a continuous metallic gold film. The nucleation/growth/coalescence process is visually noticeable as it induces a change of colour on the gold film [48]. The reaction kinetics has been optimized in order to obtain continuous gold films. The key parameters are the gold precursor concentration and the $V_{HAuCl_4}/V_{H_2O_2}$ ratio. The thickness of the gold film mostly depends on the reaction time [49, 50]. We have set this parameter to 2 min, in order to obtain continuous conductive metallic films of controlled thickness (20 nm) between each PS assembly layers. Similar results have been obtained elsewhere [40]. In this work, Hu et al. employed a multistep process to ensure adherence of gold nanoparticles to the substrate. Their process consisted in functionalizing the glass surface with organic linkers (APTMS), followed by the use of citrate-stabilized gold nanoparticles as nucleation sites. The functionalizing step lasted 16 hours under inert atmosphere, followed by the immersion during 6 hours in the gold-citrate solution. The alternative process we are presenting is a time-efficient one-step method based on a sol-gel process.

3.4. XRD Characterization. The Au/ZrO_2 seed layer was analyzed by Grazing Incidence X-Ray Diffraction (GIXRD) (Figure 4(a)). The diagrams were recorded with a Bruker AXS D8 diffractometer using a Cu K_α radiation source (40 kV and 40 mA) and equipped with a Lynxeye XE 1D detector. Experiments were carried out between $2\theta = 25^\circ$ and 50°. The angle of incidence was fixed at 2°. The presence of a large peak on the diagram between $2\theta = 24^\circ$ and 33° is characteristic of the amorphous phase of the zirconia. This observation is consistent with the fact that ZrO_2 presents a crystal structure only at high temperature [51] and remains amorphous at RT. The low-intensity peak situated at $2\theta = 38.65^\circ$ could be attributed to the cubic gold crystal structure. In order to confirm the presence of gold nanoparticles embedded in the ZrO_2 matrix, the film was treated at 1200°C under air (Figure 4(b)). One can observe the characteristic peaks of the monoclinic ZrO_2 crystal structure at $2\theta = 24.00^\circ$; 24.36°; 28.00°; 31.46°; 34.14°; 34.39°; 35.28°; 35.87°; 38.54°; 38.80°; 39.41°; 39.95°; 40.70°; 41.13°; 41.37°; 44.80°; 45.49°; 48.90°; and 49.24° according to the ICDD card reference 00-037-1484. The presence of gold particles is also evidenced by the diffraction peaks at $2\theta = 38.18^\circ$ and $2\theta = 44.39^\circ$ (ICDD card reference 00-004-0784). No additional phase is observed. The GIXRD diagram of the Au/PS 10-layered film (Figure 4(c)) exhibits diffraction peaks at $2\theta = 38.18^\circ$ and $2\theta = 44.39^\circ$ corresponding to the (111) and (200) lattice planes of the cubic gold crystal structure (ICDD card reference 00-004-0784). The relative intensity of the diffraction peaks shows that there

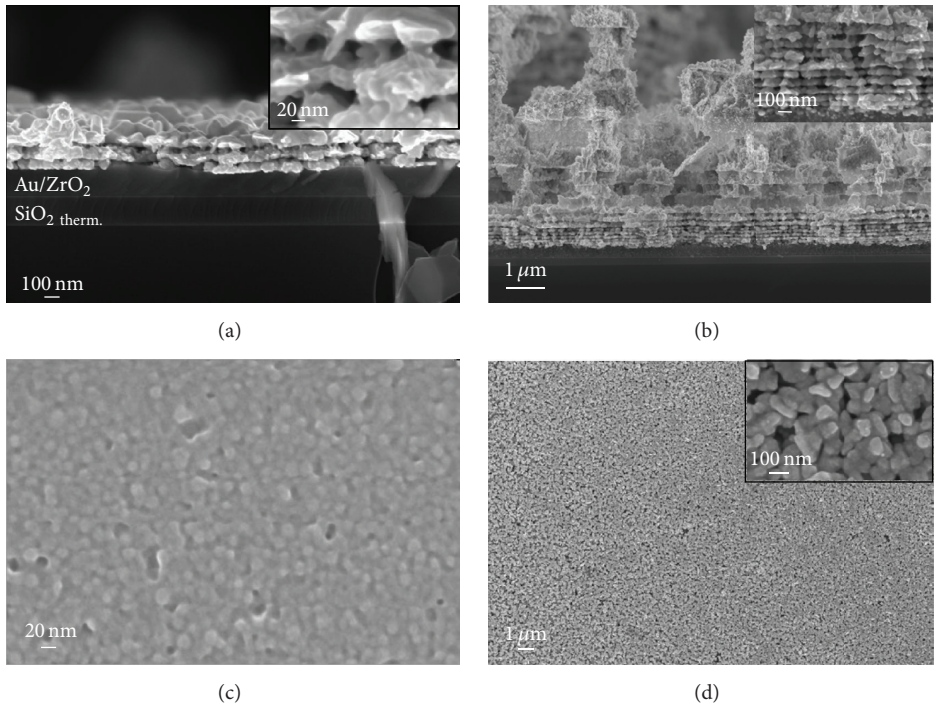

Figure 5: SEM micrographs of (a) PGF after two PS layers, (b) PGF after twenty PS layers, (c) PS beads assembly, and (d) top view of the ten PS layers film.

is no preferential orientation during the formation of the gold film onto the silicon substrate. No additional crystal phase is observed.

3.5. SEM Analysis. Scanning Electron Microscopy (SEM) analyses were carried out using a Zeiss Ultra 55. Images of the porous gold films at different steps of the deposition process are shown in Figure 5. The different layers deposited during the process can be seen in Figure 5(a). The lower 200 nm thick layer corresponds to the thermally oxidized silicon ($SiO_{2\,\mathrm{therm.}}$), coated with the 300 nm thick seed layer (Au/ZrO_2) on top of which we find the PGF. This porous film is composed of two layers of PS beads assemblies coated with 20 nm thick gold thin films. The inset of Figure 5(a) (zoom on the porous film) shows the porosity created within the film. The hole size fits the diameter of the PS beads obtained by DLS measurements. The deposition of ten successive PS beads assemblies/gold thin film is represented in the inset of Figure 5(b). No change in the structure of the overall film was noticed. The pore size and the gold thin film thicknesses stayed unchanged during all the process. At this point, the porous gold film reaches a thickness of about 1.2 μm, while presenting no delamination. In order to increase the thickness of the porous gold film, the deposition of 10 additional Au/PS layers was experimented. The first 10 Au/PS layers are uniformly deposited. However, the deposition of the last 10 Au/PS layers revealed the presence of large (about 3.6 μm thick) blocks of stacked alternative Au/PS layers (Figure 5(b)). This behaviour may be related to internal mechanical stress within the material. Experimentally, we observed that the 10 upper layers are thicker and thicker as we carry on with the PS beads deposition/electroless plating steps. We can deduce from these observations that we have reached a limit in the PGF growth by electroless deposition after 10 successive Au/PS layers. The same result was obtained after each experiment conducted, showing the reproducibility of the structure beyond the critical point. A SEM picture of the PS beads assembly is presented in Figure 5(c). We can notice that the PS beads are uniformly deposited on the gold-coated substrate. Figure 5(d) shows the surface state of the 10-layered film and a zoom on this surface state in the inset. The final layer is homogeneous, continuous, and crackless and contains low porosity. The gold layers between porous layers are connected altogether and are about 20 nm thick. Such a thickness allows the film to be continuous and conductive. All the pores of the material are considered to be interconnected since there are no remaining PS beads after toluene treatment, even the ones situated close to the substrate.

3.6. AFM Analysis. Atomic-Force Microscopy (AFM) analyses were performed using a Bruker Edge atomic force microscope. Figures 6(a) and 6(b) show the 2D and 3D 1 μm $\times$ 1 μm images, respectively, of the PS beads assembly. From these figures, we can observe that the PS beads are spherical and form a continuous film. The homogeneity of contrast highlights the fact that the PS beads composing the film are on the same level. The absence of volume effect, as the layer exhibits a high density, is confirmed by the extracted profile (based on the white line from Figure 6(a)) (Figure 6(c)). The RMS roughness calculated (from Figure 6(a)) is 6.64 nm,

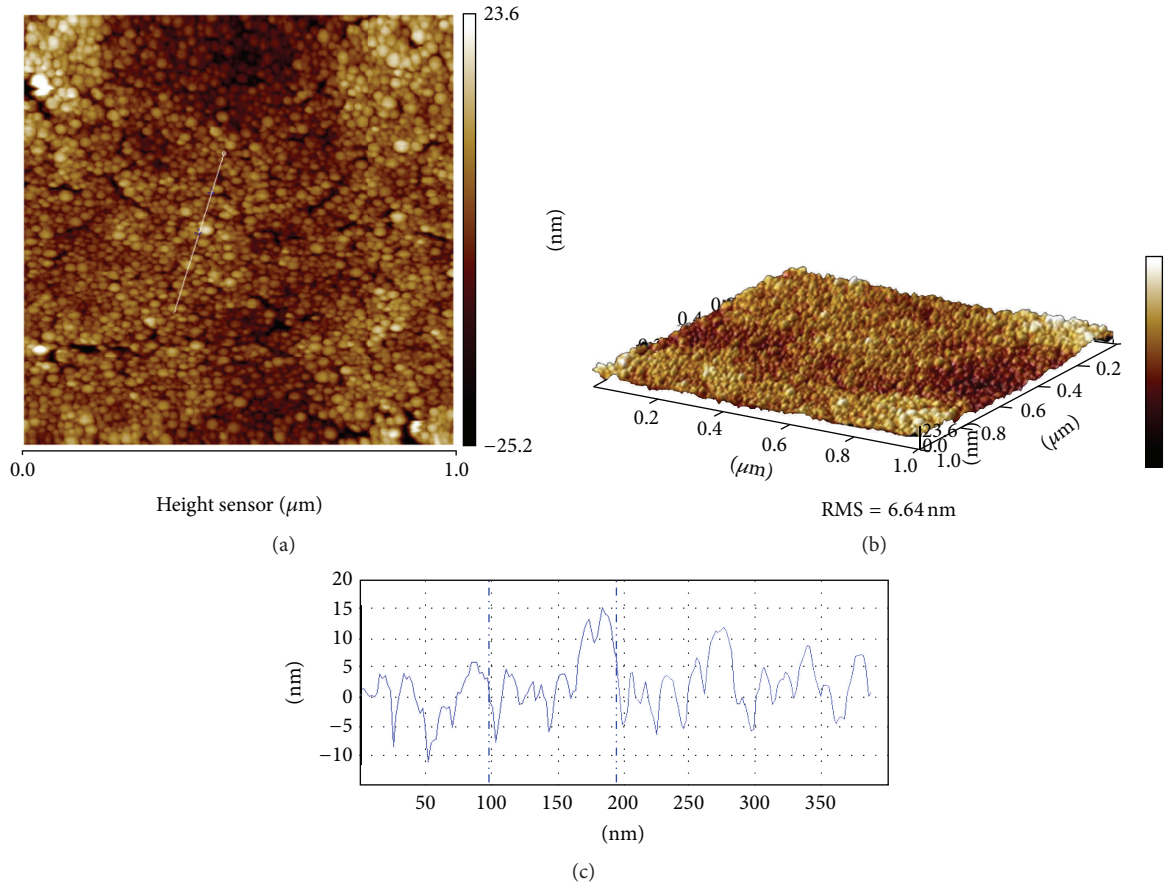

Figure 6: (a) AFM 2D 1 μm × 1 μm image, (b) AFM 3D 1 μm × 1 μm image, and (c) extracted line profiles from the 1 μm × 1 μm image.

which is low. This result shows that the distribution of the PS beads is homogeneous. The morphology of the PS beads assembly studied by AFM confirmed the observations previously made by SEM (Figure 5(c)).

3.7. Krypton Adsorption-Desorption Isotherms. The Brunauer-Emmett-Teller (BET) specific surface areas (S_{BET}) were determined from krypton adsorption-desorption at 77.35 K using a Bel Japan Belsorp Max Instrument. Prior to the experiments, the samples were outgassed at RT for several hours under secondary vacuum. The PGFs exhibit a S_{BET} of 4 $m^2 \cdot g^{-1}$, which is considered to be high for such a material [1, 37]. However, we were not able to determine an accurate pore size as the sample mass characterized was too low (3.3 mg compared to the few hundred milligrams commonly required).

3.8. Electrical Characterization. The electrical conductivity of a 1 μm thick porous gold thin film has been measured using a Jandel RM2 four-point probes system (Figure 7). The probes exhibit a 1.0 mm spacing and a 125 μm tip radius. The value of the conductivity has been assessed to be $2 \pm 0.2 \times 10^6$ $(\Omega \cdot cm)^{-1}$, which is about 20 times less than dense gold. Similar results of PGFs conductivity have been found in the literature. Maaroof et al. stated that the electrical conductivity

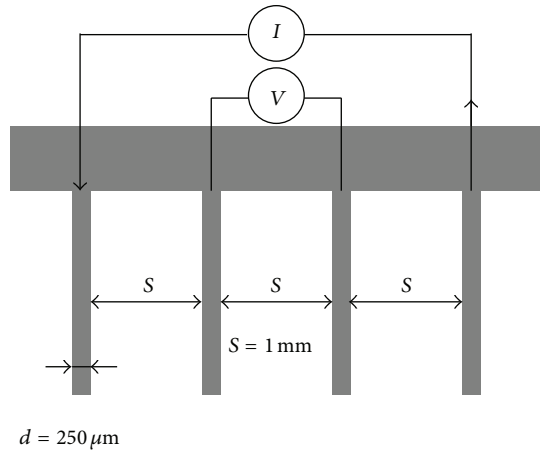

Figure 7: Drawing of a four-point probes system.

of porous gold films is in the range 1×10^5–3×10^6 $(\Omega \cdot m)^{-1}$ [1]. The decrease in the conductivity value is due to the presence of pores in the material and hence the presence of air, which is an insulating medium. As a comparison, the carbon exhibits an electrical conductivity of 6.1×10^4 $(\Omega \cdot cm)^{-1}$.

4. Conclusion

The fabrication of porous gold films by an original "bottom-up" approach through combined PS beads templating and gold electroless deposition methods has been achieved. All the techniques employed in the fabrication of the PGFs are totally wet-chemistry processes. The deposition of an original sol-gel-based Au/ZrO_2 adhesion/seed layer onto a silicon substrate has been presented in this paper. Dip-coating and drying parameters have been optimized in order to deposit a uniform, continuous, and crackless film. The ZrO_2 matrix anchors the Au nanoparticles to the substrate and prevents the delamination of the final material (PGF) up to a thickness of 1.2 μm. Simultaneously, the gold nanoparticles embedded in the ZrO_2 matrix act as growth seeds for the following gold electroless deposition. An autoassembly of PS beads (template) has been deposited onto the Au/ZrO_2 film by dip-coating technique. Gold electroless deposition kinetics parameters have been optimized in order to obtain continuous conductive gold thin films of controlled thickness between PS layers. The process described is conducted several times and the PS layers are removed by dissolution. SEM pictures showed a three-dimensional network of interconnected and size-tailored 20 nm wide pores separated by 20 nm thick continuous gold layers. Krypton adsorption-desorption isotherms demonstrated a specific surface area (S_{BET}) of about 4 $m^2 \cdot g^{-1}$. The fabrication process described in this paper allows the deposition of a material exhibiting at the same time a good conductivity value (2×10^6 $(\Omega \cdot cm)^{-1}$) and well-defined 20 nm wide pores. Such material is a promising candidate for electric double-layer capacitor electrodes or bio-/chemical sensors, for instance.

Disclosure

Katarzyna Raulin is now working at Ethera, 7 Parvis Louis Néel, CS 20050, 38040 Grenoble Cedex 9.

Competing Interests

The authors declare that they have no competing interests.

Acknowledgments

This work was supported by the ERDF (European Regional Development Fund), by the Nord-Pas-de-Calais Region (France) through the CIA Project (2009–2013), and by the ANR through the INPACT Project (2014–2017) and the AMPEROR Project (2014–2017). This work was also partly supported by the Equipex FLUX through the Programme Investissements d'Avenir.

References

[1] A. I. Maaroof, M. B. Cortie, A. Gentle, and G. B. Smith, "Mesoporous gold sponge as a prototype 'metamaterial'," *Physica B: Condensed Matter*, vol. 394, no. 2, pp. 167–170, 2007.

[2] D. Van Noort and C.-F. Mandenius, "Porous gold surfaces for biosensor applications," *Biosensors and Bioelectronics*, vol. 15, no. 3-4, pp. 203–209, 2000.

[3] P. S. Liu and G. F. Chen, *Porous Materials Processing and Applications*, Elsevier Science Butterworth-Heinemann, Oxford, UK, 2014.

[4] C. Mele, M. Catalano, A. Taurino, and B. Bozzini, "Electrochemical fabrication of nanoporous gold-supported manganese oxide nanowires based on electrodeposition from eutectic urea/choline chloride ionic liquid," *Electrochimica Acta*, vol. 87, pp. 918–924, 2013.

[5] Z. Zeng, X. Long, H. Zhou, E. Guo, X. Wang, and Z. Hu, "On-chip interdigitated supercapacitor based on nanoporous gold/manganese oxide nanowires hybrid electrode," *Electrochimica Acta*, vol. 163, pp. 107–115, 2015.

[6] X. Lang, A. Hirata, T. Fujita, and M. Chen, "Nanoporous metal/oxide hybrid electrodes for electrochemical supercapacitors," *Nature Nanotechnology*, vol. 6, no. 4, pp. 232–236, 2011.

[7] T. Fujita, H. Okada, K. Koyama, K. Watanabe, S. Maekawa, and M. W. Chen, "Unusually small electrical resistance of three-dimensional nanoporous gold in external magnetic fields," *Physical Review Letters*, vol. 101, no. 16, Article ID 166601, 2008.

[8] Y. Yu, L. Gu, X. Lang et al., "Li storage in 3D nanoporous au-supported nanocrystalline tin," *Advanced Materials*, vol. 23, no. 21, pp. 2443–2447, 2011.

[9] L. C. Nagle and J. F. Rohan, "Nanoporous gold anode catalyst for direct borohydride fuel cell," *International Journal of Hydrogen Energy*, vol. 36, no. 16, pp. 10319–10326, 2011.

[10] X. B. Ge, R. Y. Wang, P. P. Liu, and Y. Ding, "Platinum-decorated nanoporous gold leaf for methanol electrooxidation," *Chemistry of Materials*, vol. 19, no. 24, pp. 5827–5829, 2007.

[11] J. Erlebacher, M. J. Aziz, A. Karma, N. Dimitrov, and K. Sieradzki, "Evolution of nanoporosity in dealloying," *Nature*, vol. 410, no. 6827, pp. 450–453, 2001.

[12] Y. Xia, W. Huang, J. Zheng, Z. Niu, and Z. Li, "Nonenzymatic amperometric response of glucose on a nanoporous gold film electrode fabricated by a rapid and simple electrochemical method," *Biosensors and Bioelectronics*, vol. 26, no. 8, pp. 3555–3561, 2011.

[13] C. S. Oh, H. Kim, S. Rengaraj, and Y. Kim, "In situ detection and removal of metal ion by porous gold electrode," *Microporous and Mesoporous Materials*, vol. 147, no. 1, pp. 1–4, 2012.

[14] H. Kim, Y. Kim, J. B. Joo, J. W. Ko, and J. Yi, "Preparation of coral-like porous gold for metal ion detection," *Microporous and Mesoporous Materials*, vol. 122, no. 1–3, pp. 283–287, 2009.

[15] G. W. Nyce, J. R. Hayes, A. V. Hamza, and J. H. Satcher, "Synthesis and characterization of hierarchical porous gold materials," *Chemistry of Materials*, vol. 19, no. 3, pp. 344–346, 2007.

[16] A. Wittstock, V. Zielasek, J. Biener, C. M. Friend, and M. Bäumer, "Nanoporous gold catalysts for selective gas-phase oxidative coupling of methanol at low temperature," *Science*, vol. 327, no. 5963, pp. 319–322, 2010.

[17] Y. Deng, W. Huang, X. Chen, and Z. Li, "Facile fabrication of nanoporous gold film electrodes," *Electrochemistry Communications*, vol. 10, no. 5, pp. 810–813, 2008.

[18] S. O. Kucheyev, J. R. Hayes, J. Biener, T. Huser, C. E. Talley, and A. V. Hamza, "Surface-enhanced Raman scattering on nanoporous Au," *Applied Physics Letters*, vol. 89, no. 5, Article ID 053102, 2006.

[19] H.-O. Lee, E.-M. Kim, H. Yu, J.-S. Jung, and W.-S. Chae, "Advanced porous gold nanofibers for highly efficient and stable molecular sensing platforms," *Nanotechnology*, vol. 20, no. 32, Article ID 325604, 2009.

[20] S. Y. Gao, H. J. Zhang, X. M. Wang et al., "Unique gold sponges: biopolymer-assisted hydrothermal synthesis and potential application as surface-enhanced Raman scattering substrates," *Nanotechnology*, vol. 16, no. 11, pp. 2530–2535, 2005.

[21] S. Cherevko and C.-H. Chung, "Direct electrodeposition of nanoporous gold with controlled multimodal pore size distribution," *Electrochemistry Communications*, vol. 13, no. 1, pp. 16–19, 2011.

[22] M. E. Cox and D. C. Dunand, "Bulk gold with hierarchical macro-, micro- and nano-porosity," *Materials Science and Engineering A*, vol. 528, no. 6, pp. 2401–2406, 2011.

[23] A. J. Forty, "Corrosion micromorphology of noble metal alloys and depletion gilding," *Nature*, vol. 282, no. 5739, pp. 597–598, 1979.

[24] Y. Ding and J. Erlebacher, "Nanoporous metals with controlled multimodal pore size distribution," *Journal of the American Chemical Society*, vol. 125, no. 26, pp. 7772–7773, 2003.

[25] K. Wagner, S. R. Brankovic, N. Dimitrov, and K. J. Sieradzki, "Dealloying below the critical potential," *Journal of the Electrochemical Society*, vol. 144, no. 10, pp. 3545–3555, 1997.

[26] Y. Sun, K. P. Kucera, S. A. Burger, and T. John Balk, "Microstructure, stability and thermomechanical behavior of crack-free thin films of nanoporous gold," *Scripta Materialia*, vol. 58, no. 11, pp. 1018–1021, 2008.

[27] A. J. Forty and P. Durkin, "Micromorphological study of the dissolution of silver-gold alloys in nitric acid," *Philosophical Magazine A*, vol. 42, no. 3, pp. 295–318, 1980.

[28] I. C. Oppenheim, D. J. Trevor, C. E. D. Chidsey, P. L. Trevor, and K. Sieradzki, "In situ scanning tunneling microscopy of corrosion of silver-gold alloys," *Science*, vol. 254, no. 5032, pp. 687–689, 1991.

[29] T. Bryce C, S. Stephen A III, and E. P. Luther, "Nanoporous metal foams," *Angewandte Chemie—International Edition*, vol. 49, no. 27, pp. 4544–4565, 2010.

[30] O. D. Velev and A. M. Lenhoff, "Colloidal crystals as templates for porous materials," *Current Opinion in Colloid & Interface Science*, vol. 5, no. 1-2, pp. 56–63, 2000.

[31] P. Jiang, J. Cizeron, J. F. Bertone, and V. L. Colvin, "Preparation of macroporous metal films from colloidal crystals," *Journal of the American Chemical Society*, vol. 121, no. 34, pp. 7957–7958, 1999.

[32] R. Szamocki, S. Reculusa, S. Ravaine, P. N. Bartlett, A. Kuhn, and R. Hempelmann, "Tailored mesostructuring and biofunctionalization of gold for increased electroactivity," *Angewandte Chemie—International Edition*, vol. 45, no. 8, pp. 1317–1321, 2006.

[33] O. D. Velev, P. M. Tessier, A. M. Lenhoff, and E. W. Kaler, "A class of porous metallic nanostructures," *Nature*, vol. 401, no. 6753, p. 548, 1999.

[34] Y. Bai, W. Yang, Y. Sun, and C. Sun, "Enzyme-free glucose sensor based on a three-dimensional gold film electrode," *Sensors and Actuators B: Chemical*, vol. 134, no. 2, pp. 471–476, 2008.

[35] H. Kim and Y. Kim, "Preparation of nanoporous gold using PS bead, Ludox and nanoporous alumina as physical templates," *Current Applied Physics*, vol. 9, no. 1, pp. S88–S90, 2009.

[36] H. Zhang, I. Hussain, M. Brust, and A. I. Cooper, "Emulsion-templated gold beads using gold nanoparticles as building blocks," *Advanced Materials*, vol. 16, no. 1, pp. 27–30, 2004.

[37] H. Du Toit and M. Di Lorenzo, "Electrodeposited highly porous gold microelectrodes for the direct electrocatalytic oxidation of aqueous glucose," *Sensors and Actuators B: Chemical*, vol. 192, pp. 725–729, 2014.

[38] R. Seshadri and F. C. Meldrum, "Bioskeletons as templates for ordered, macroporous structures," *Advanced Materials*, vol. 12, no. 15, pp. 1149–1151, 2000.

[39] F. C. Meldrum and R. Seshadri, "Porous gold structures through templating by echinoid skeletal plates," *Chemical Communications*, no. 1, pp. 29–30, 2000.

[40] J. Hu, W. Li, J. Chen, X. Zhang, and X. Zhao, "Novel plating solution for electroless deposition of gold film onto glass surface," *Surface & Coatings Technology*, vol. 202, no. 13, pp. 2922–2926, 2008.

[41] A. Le Rouge, H. El Hamzaoui, B. Capoen et al., "Synthesis and nonlinear optical properties of zirconia-protected gold nanoparticles embedded in sol–gel derived silica glass," *Materials Research Express*, vol. 2, no. 5, Article ID 055009, 2015.

[42] J. C. Debsikdar, "Transparent zirconia gel-monolith from zirconium alkoxide," *Journal of Non-Crystalline Solids*, vol. 86, no. 1-2, pp. 231–240, 1986.

[43] K. Liu and Z. Wang, "A novel method for preparing monodispersed polystyrene nanoparticles," *Frontiers of Chemistry in China*, vol. 2, no. 1, pp. 17–20, 2007.

[44] T. Ung, L. M. Liz-Marzán, and P. Mulvaney, "Gold nanoparticle thin films," *Colloids and Surfaces A: Physicochemical and Engineering Aspects*, vol. 202, no. 2-3, pp. 119–126, 2002.

[45] Y. Fu, Z. Jin, Z. Liu, and W. Li, "Preparation of ordered porous SnO_2 films by dip-drawing method with PS colloid crystal templates," *Journal of the European Ceramic Society*, vol. 27, no. 5, pp. 2223–2228, 2007.

[46] J. Zhang, Z. Chen, Z. Wang, W. Zhang, and N. Ming, "Preparation of monodisperse polystyrene spheres in aqueous alcohol system," *Materials Letters*, vol. 57, no. 28, pp. 4466–4470, 2003.

[47] Z. Liu, J. Ya, Y. Xin, J. Ma, and C. Zhou, "Assembly of polystyrene colloidal crystal templates by a dip-drawing method," *Journal of Crystal Growth*, vol. 297, no. 1, pp. 223–227, 2006.

[48] G. W. Qin, J. Liu, T. Balaji et al., "A facile and template-free method to prepare mesoporous gold sponge and its pore size control," *The Journal of Physical Chemistry C*, vol. 112, no. 28, pp. 10352–10358, 2008.

[49] L. A. Nagahara, T. Ohmori, K. Hashimoto, and A. Fujishima, "The influence of hydrofluoric acid concentration on electroless copper deposition onto silicon," *Journal of Electroanalytical Chemistry*, vol. 333, no. 1-2, pp. 363–369, 1992.

[50] L. A. Nagahara, T. Ohmori, K. Hashimoto, and A. Fujishima, "Effects of HF solution in the electroless deposition process on silicon surfaces," *Journal of Vacuum Science & Technology A*, vol. 11, no. 4, pp. 763–767, 1993.

[51] J. D. McCullough and K. N. Trueblood, "The crystal structure of baddeleyite (monoclinic ZrO_2)," *Acta Crystallographica*, vol. 12, no. 7, pp. 507–511, 1959.